

Ion chemistry in the coma of comet 67P near perihelion

S. A. Fuselier,^{1,2★} K. Altwegg,³ H. Balsiger,³ J. J. Berthelier,⁴ A. Beth,⁵ A. Bieler,^{3,6} C. Briois,⁷ T. W. Broiles,¹ J. L. Burch,¹ U. Calmonte,³ G. Cessateur,⁸ M. Combi,⁵ J. De Keyser,⁸ B. Fiethe,⁹ M. Galand,^{5★} S. Gasc,³ T. I. Gombosi,⁶ H. Gunell,⁸ K. C. Hansen,⁶ M. Hässig,¹ K. L. Heritier,⁵ A. Korth,¹⁰ L. Le Roy,³ A. Luspay-Kuti,¹ U. Mall,¹⁰ K. E. Mandt,^{1,2} S. M. Petrinec,¹¹ H. Rème,^{12,13} M. Rinaldi,¹ M. Rubin,^{3★} T. Sémon,³ K. J. Trattner,¹⁴ C.-Y. Tzou,³ E. Vigren,¹⁵ J. H. Waite^{1,2} and P. Würz³

¹Southwest Research Institute, 6220 Culebra Road, San Antonio, Texas, 78228, USA

²Department of Physics and Astronomy, University of Texas at San Antonio, San Antonio, Texas, USA

³Physikalisches Institut, University of Bern, Sidlerstrasse 5, CH-3012 Bern, Switzerland

⁴LATMOS 4 Avenue de Neptune, F-94100 SAINT-MAUR, France

⁵Space and Atmospheric Physics Group, Department of Physics, Imperial College London, Prince Consort Road, London, SW7 2AZ, UK

⁶Department of Atmospheric, Oceanic and Space Sciences, University of Michigan, 2455 Hayward, Ann Arbor, MI 48109, USA

⁷Laboratoire de Physique et Chimie de l'Environnement et de l'Espace (LPC2E), F-45071 UMR 6115 CNRS–Université d'Orléans, France

⁸Belgian Institute for Space Aeronomy (BIRA-IASB), Ringlaan 3, B-1180, Brussels, Belgium

⁹Institute of Computer and Network Engineering (IDA), TU Braunschweig, Hans-Sommer-Straße 66, D-38106 Braunschweig, Germany

¹⁰Max-Planck-Institut für Sonnensystemforschung, Justus-von-Liebig-Weg 3, D-37077 Göttingen, Germany

¹¹Lockheed Martin Advanced Technology Center, Palo Alto, CA 94304, USA

¹²Université de Toulouse, UPS-OMP, IRAP, F-31400 Toulouse, France

¹³CNRS, IRAP, 9 avenue du colonel Roche, BP 44346, F-31028 Toulouse cedex 4, France

¹⁴Laboratory of Atmospheric and Space Physics, University of Colorado, Boulder, CO 80303, USA

¹⁵Swedish Institute of Space Physics, SE-75121 Uppsala, Sweden

Accepted 2016 August 23. Received 2016 August 22; in original form 2016 May 31

ABSTRACT

The coma and the comet–solar wind interaction of comet 67P/Churyumov–Gerasimenko changed dramatically from the initial *Rosetta* spacecraft encounter in 2014 August through perihelion in 2015 August. Just before equinox (at 1.6 au from the Sun), the solar wind signal disappeared and two regions of different cometary ion characteristics were observed. These ‘outer’ and ‘inner’ regions have cometary ion characteristics similar to outside and inside the ion pileup region observed during the Giotto approach to comet 1P/Halley. *Rosetta*/Double-Focusing Mass Spectrometer ion mass spectrometer observations are used here to investigate the $\text{H}_3\text{O}^+/\text{H}_2\text{O}^+$ ratio in the outer and inner regions at 67P/Churyumov–Gerasimenko. The $\text{H}_3\text{O}^+/\text{H}_2\text{O}^+$ ratio and the H_3O^+ signal are observed to increase in the transition from the outer to the inner region and the H_3O^+ signal appears to be weakly correlated with cometary ion energy. These ion composition changes are similar to the ones observed during the 1P/Halley flyby. Modelling is used to determine the importance of neutral composition and transport of neutrals and ions away from the nucleus. This modelling demonstrates that changes in the $\text{H}_3\text{O}^+/\text{H}_2\text{O}^+$ ratio appear to be driven largely by transport properties and only weakly by neutral composition in the coma.

Key words: plasmas – solar wind – comets: general – comets: individual.

1 INTRODUCTION TO ION-NEUTRAL CHEMISTRY IN COMETARY COMAE

As comets approach the Sun and warm up, they release water and other volatiles that produce an extended atmosphere or coma of

neutrals, ions, and electrons. The solar wind interaction with this atmosphere creates boundaries and regions within the coma, such as those observed during the fly-bys of comet 1P/Halley (hereafter referred to simply as Halley; e.g. see the review by Coates 1997).

Two important boundaries and regions observed during the fly-bys of Halley were the so-called ion pile-up region (Balsiger et al. 1986; Gringauz et al. 1986; Vaisberg et al. 1987; Schwenn et al. 1988) and the contact surface/diamagnetic cavity (Neubauer

* E-mail: sfuselier@swri.edu (SAF); m.galand@imperial.ac.uk (MG); martin.rubin@space.unibe.ch (MR)

et al. 1986). In the ion pile-up region, the density increased with decreasing distance to the comet. At a point where the ion bulk flow velocity decreased, the ion composition changed (Schwenn et al. 1988). At the contact surface, the magnetic field and the plasma upstream of the nucleus were excluded from the diamagnetic cavity (Neubauer et al. 1986) that formed around the nucleus and the low-energy ion outflow velocity decreased (Schwenn et al. 1988). Inside the diamagnetic cavity, only the outflowing cometary neutrals and ions (created by ionization of a fraction of the neutrals) were observed (Balsiger et al. 1986; Schwenn et al. 1988).

Rosetta encountered comet 67P/Churyumov–Gerasimenko (hereafter referred to simply as 67P) at a distance of ~ 3 au from the Sun and observed a weaker comet–solar wind interaction. At ~ 3 au, there was minimal charge exchange loss of the solar wind (Burch et al. 2015), and slight deflection of the solar wind due to the mass loading by cometary ions (Broiles et al. 2015; Behar et al. 2016). Because the outgassing rate was low ($\sim 10^{26}$ molecules s^{-1}), all outgassing values presented here are from Hansen et al. 2016 and assume an outgassing neutral velocity of 700 $m s^{-1}$, the solar wind had direct access to the nucleus and solar wind impact on the surface caused sputtering of non-volatile elements from the surface (Wurz et al. 2015). Also, there was minimal ion-neutral chemistry, that was reasonably well described by a simple model that allowed only one ion-neutral interaction between the ionized and neutral species as they propagated across the ~ 30 km gap that separated the nucleus and the spacecraft (Fuselier et al. 2015).

With the increased outgassing of 67P closer to the Sun, some boundaries and regions developed. From its vantage point at about 100–400 km from the nucleus, *Rosetta* observed the disappearance of the solar wind (Mandt et al. 2016), possibly because it was deflected away from the comet (Broiles et al. 2015; Behar et al. 2016). Two regions of relatively higher and lower total ion energy were observed after the solar wind disappeared (Mandt et al. 2016). The ‘inner region’ had lower average water-group ion energies (~ 1 –10 eV), higher electron densities, and lower magnetic field magnitudes, while the ‘outer region’ had higher average water-group ion energies (tens of eV to ~ 100 eV), lower electron densities, and higher magnetic field magnitudes. These average ion energies are, in reality, lower because the spacecraft potential was typically negative. The inner region had some characteristics of the ion pile-up region observed at comet Halley (Mandt et al. 2016). The ‘boundary’, or transition between these two regions was sometimes narrow and at other times very broad. The distance of this transition from the nucleus appeared to depend on the neutral outgassing rate, but also to be influenced by solar wind dynamic pressure. Comparing the observed boundary location with the predicted location of an ion-neutral collisionopause suggests that the observed boundary might be the point at which the collisions begin to dominate the plasma dynamics and keep the ion bulk flow velocity close to the neutral bulk flow velocity.

In addition to these regions, there is evidence of at least a transient diamagnetic cavity very near to the comet (Goetz et al. 2016). Thus, in close proximity of the nucleus, *Rosetta* observed some regions that appear to be similar in character to regions observed at Halley. Because the outgassing rate of 67P was significantly lower than that of Halley, these regions are much closer to the comet nucleus than those observed at Halley.

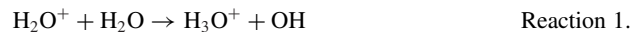
In the ion pile-up region at comet Halley, the densities of ions with mass/charge 16 through 19 u/e increased as the comet was approached. Moreover, the mass 19/mass 18 ratio (H_3O^+/H_2O^+) increased from less than 1–20 000 km from the comet to a peak value of about 5–6 at 10 000 km from the comet. Inside this distance,

the ratio dropped abruptly, but remained about 3 (Altwegg et al. 1993). These distances are very large compared to the distance of about 100–300 km between *Rosetta* and comet 67P from equinox (2015 May) to perihelion (2015 August 13). However, the similarity between the inner and outer ion regions at 67P and the Giotto observations inside and outside the ion pile-up region at P/Halley suggests that the H_3O^+/H_2O^+ ratio may change in a similar manner at the two comets. In a broader context, it is important to understand how the H_3O^+/H_2O^+ ratio evolved as 67P became more active and the ion-neutral chemistry became more complex.

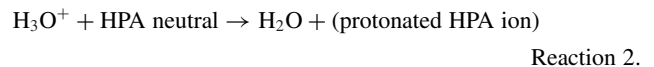
2 FORMATION OF H_2O^+ , H_3O^+ , AND THE H_3O^+/H_2O^+ RATIO

The H_3O^+/H_2O^+ ratio in the coma of comets is a balance between production and loss of the primary parent ion, H_2O^+ , and the daughter ion, H_3O^+ , formed by protonation from mostly neutral H_2O . Production of H_3O^+ is directly linked to the outgassing of H_2O and creation of H_2O^+ . Far from the Sun, neutral H_2O outgassing is low ($\sim 10^{26}$ molecules s^{-1} at ~ 3 au for comet 67P) and H_2O^+ is produced by photoionization, ion charge exchange with solar wind ions, and electron impact ionization. All three of these ionization processes are relatively weak because the photoionization rate decreases as $1/R^2$ from the Sun, the solar wind ion density decreases with increasing distance from the Sun (approximately as $1/R^2$; e.g. Richardson, Paularena & Gazis 1995), and the energetic electron flux, (i.e., electrons with energies of 100s of eV) is low (Broiles et al. 2016). Overall, photoionization dominates over the summer hemisphere and electron impact ionization is significant over the winter hemisphere (Galand et al. 2016).

H_3O^+ is produced primarily by the following ion-neutral reaction in the coma:



H_3O^+ is primarily destroyed by the following ion-neutral reaction with a high proton affinity (HPA) neutral in the coma:



The primary (HPA) neutral in the coma that destroys H_3O^+ is NH_3 , and the reaction produces NH_4^+ (Beth et al. 2016); however, there are several other candidate HPA neutrals. Thus, the detection of cometary NH_4^+ demonstrates that this type of secondary ion-neutral reaction occurs in the coma. H_3O^+ is also destroyed in ion–electron recombination when there are sufficient numbers of low-energy electrons present in the coma (Vigren & Galand 2013).

The coma of comets is far from static and far from equilibrium. Neutrals continually outgas from the nucleus and ions are ‘picked up’ by incoming solar wind or other cometary ions. Therefore, number densities of H_3O^+ and H_2O^+ and their ratio are strongly influenced by how fast neutrals leave the nucleus and how fast newly created ions are picked up.

Far from the Sun, the coma was thin and cometary ions were rapidly accelerated in the coma. In addition, the *Rosetta* spacecraft was quite close to the 67P (within 30 km) and ions had little time to interact with neutrals or other ions before they convected past the spacecraft.

Closer to the Sun, neutral outgassing is higher (between 10^{27} at equinox and 10^{28} mol s^{-1} at perihelion) and photoionization rates are higher and the mean free path is of the order of 1 km near the nucleus. The loss of the solar wind before equinox (Mandt et al. 2016)

indicates that photoionization and possibly electron impact ionization are the primary ion production processes. Vigren & Galand (2013) argued that photoionization dominates in the diamagnetic region. Because the solar wind is no longer present, estimating the pickup time-scales for newly created cometary ions is more complicated. Pickup time-scales become important because the *Rosetta* spacecraft was considerably farther away from the comet (about 170 versus ~ 30 km near 3 au from the Sun) between equinox (1.6 au) and perihelion (1.3 au). The increased propagation time between the comet and the spacecraft combined with the higher ion and neutral densities (and shorter mean free path) dictate considerably more complex ion-neutral chemistry.

The purpose of this paper is to present observations of the $\text{H}_3\text{O}^+/\text{H}_2\text{O}^+$ ratio in the coma of 67P near perihelion (i.e. 1.3 au). These observations are discussed in context with observed regions near the comet nucleus in an attempt to compare the properties of these regions with the observations made in the ion pile-up region at Halley. An ionospheric model is used to determine the relative importance of outgassing rates and neutral composition on the $\text{H}_3\text{O}^+/\text{H}_2\text{O}^+$ ratio.

3 INSTRUMENTATION AND DATA

Ion and neutral composition observations in this paper are from the *Rosetta* Orbiter Spectrometer for Ion and Neutral Analysis (ROSINA)/Double-Focusing Mass Spectrometer (DFMS). The instrument details of this high-resolution mass spectrometer are provided by Balsiger et al. (2007) and the use of this mass spectrometer for ion measurements is described by Fuselier et al. (2015). One important feature of DFMS that is pertinent to the observations presented here is that it measures both ions and neutrals, but not simultaneously. Ion measurements were scheduled and performed periodically during the approach to perihelion. The observations in Section 4 are from two periods near perihelion when a sufficient number of ion mass spectra were obtained. Neutrals were measured between these two periods. A second feature of DFMS that is pertinent to the observations presented here is that the field of view is very narrow and the energy range is limited to energies below about 45 eV (Balsiger et al. 2007). When DFMS points are close to nadir, it almost exclusively measures newly created ions propagating radially away from the nucleus. Because the field of view is so narrow, measured ion densities are only a small fraction of the total local ion densities in the coma. Therefore, ion densities in arbitrary units and the $\text{H}_3\text{O}^+/\text{H}_2\text{O}^+$ ratio are used here to describe the ion composition of the coma from this spectrometer.

In addition to composition measurements from ROSINA/DFMS, the ROSINA COMet Pressure Sensor (COPS) is used to determine the total neutral number density at the spacecraft. The density is computed from the COPS nude gauge measurements assuming that the dominant neutral species is H_2O , which is a reasonable assumption for the period near perihelion (e.g. Fougere et al. 2016).

Energetic ion measurements in this paper are from the *Rosetta* Plasma Consortium/Ion and Electron Sensor (IES). Details of this sensor are in Burch et al. (2007). IES is used here to investigate the correlation between the energetic ion measurements (between 10 eV and 22 keV) and the $\text{H}_3\text{O}^+/\text{H}_2\text{O}^+$ ratio measured by DFMS. At low energies, cometary ions are affected by the spacecraft potential; since the spacecraft is often negatively charged, the energy measured by IES is typically higher than the actual ion energy.

Table 1. General parameters from two periods near perihelion.

Interval	2015 July 5–9	2015 July 21–25
Comet distance to Sun	1.33–1.32 au	1.28–1.26 au
S/C distance to comet	170–150 km	170–175 km

4 OBSERVATIONS

The two intervals selected for this study are from 2015 July 5 to 9 and 21 to 25. The Sun–comet distance, the comet–spacecraft distance, and the outgassing rate (from Hansen et al. 2016) for these two intervals are listed in Table 1. To illustrate the basic DFMS data product, Figs 1 and 2 show representative ion mass spectra from early and late in the first interval, respectively. Mass spectra like the ones in Figs 1 and 2 were used to compute the $\text{H}_3\text{O}^+/\text{H}_2\text{O}^+$ ratios that are used later in this section.

The top panel in Fig. 1 shows the H_2O^+ peak. The possible ions located at mass/charge 18 (all mass/charge values here are u/e) are limited to H_2O^+ , NH_4^+ , and several rare, very low-density ion isotopes such as $^{17}\text{OH}^+$ and $^{18}\text{O}^+$. The low-density isotopes are well separated from H_2O^+ in DFMS high-mass resolution measurements and the lack of evidence of peaks above the background indicates that the H_2O^+ peak is well isolated in the spectrum in the top panel of Fig. 1. The only ion with possible substantial signal is NH_4^+ , which would occur near mass/charge 18.04 in Fig. 1 and is therefore also well separated from the H_2O^+ peak. The bottom panel shows the H_3O^+ peak. Like the mass/charge 18 in the top panel, there are several rare, very low-density ion isotopes such as HDO^+ and $\text{H}_2^{17}\text{O}^+$ at mass/charge 19. These isotopes in the mass/charge 19 spectrum are close to the H_3O^+ peak in this high-resolution spectrum; however, their densities are much too low to contribute to the H_3O^+ peak near mass/charge 19.02. Furthermore, there is no peak at mass/charge 20 that would correspond to H_2DO^+ or $\text{H}_2^{18}\text{O}^+$. Comparing the peaks in the top and bottom panels of Fig. 1, the H_2O^+ peak is higher than the H_3O^+ peak, and therefore the $\text{H}_3\text{O}^+/\text{H}_2\text{O}^+$ ratio is less than 1. The ratios are calculated using the fits to the entire distribution shown by the green curve, excluding background. These fits ignore slight differences in the transmission of H_3O^+ and H_2O^+ in DFMS.

Fig. 2 shows representative ion mass spectra from later in the first time interval. The format is the same as in Fig. 1. The top panel shows two well-separated peaks. Based on the location and separation of these peaks, they are identified as H_2O^+ and NH_4^+ , respectively. The discovery of NH_4^+ in the coma is presented in Beth et al. (2016). The bottom panel shows the single H_3O^+ peak. In Fig. 2, the H_3O^+ peak is considerably higher than the H_2O^+ peak, and therefore the $\text{H}_3\text{O}^+/\text{H}_2\text{O}^+$ ratio is significantly larger than 1.

Fig. 3 compares $\text{H}_3\text{O}^+/\text{H}_2\text{O}^+$ ratios, the H_3O^+ signal on the DFMS detector (ions collected in the 20 s sample time), and the running average ion energies measured by IES during the first interval from 2015 July 5 to 9. The ion energy is computed from the bulk velocity of the distribution function and this energy is smoothed using a 5-point or 17 min running average to produce the average ion energies in Fig. 3. For this interval, the spacecraft transitioned between the two ion regions is identified by Mandt et al. (2016). The average ion energy (bottom panel) in the outer region was between 20 and 80 eV and the average ion energy in the inner region was between about 2 and 10 eV. The transition occurred on 2015 July 5 near 12 UT. Characteristic of many of these transitions from the outer to inner ion region, the change in the average ion energy and therefore the transition itself is not necessarily abrupt. Furthermore, there are differences in the average ion energy within

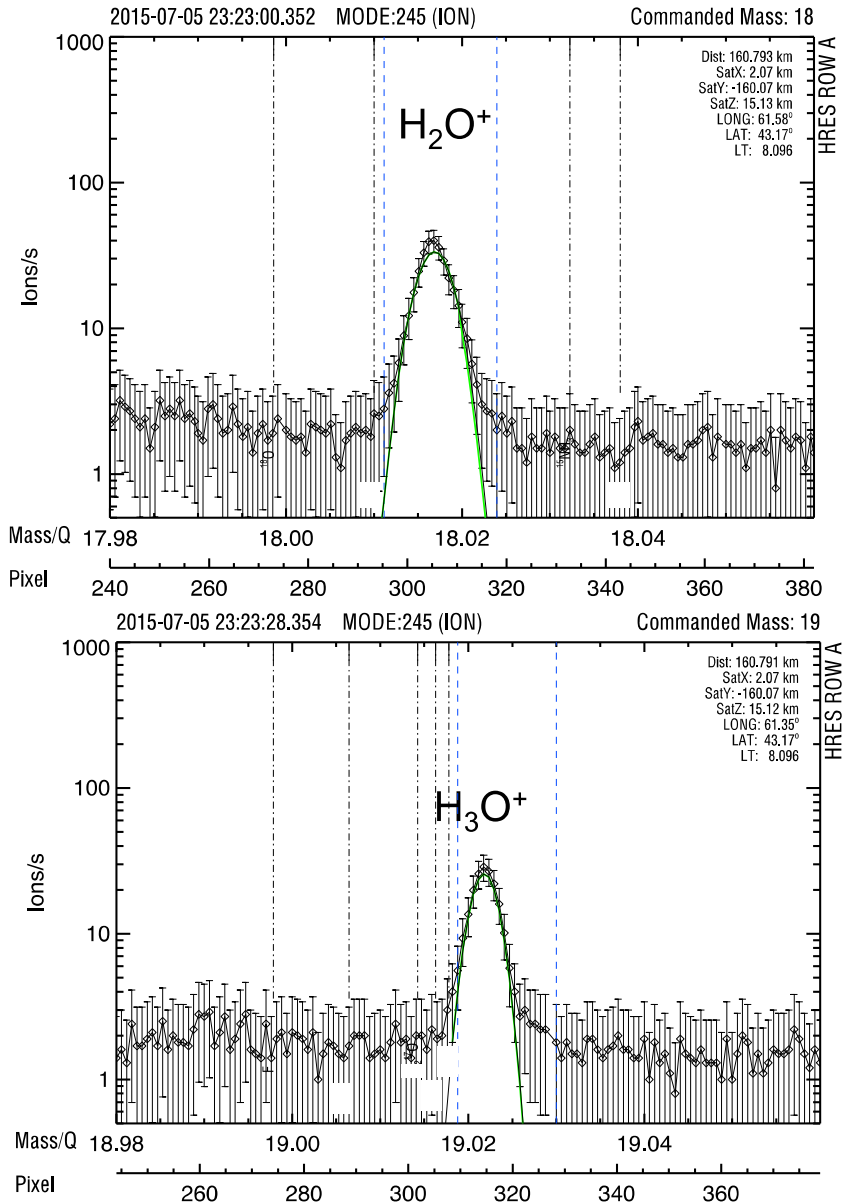


Figure 1. DFMS high-mass resolution ion observations on 2015 July 5 (near perihelion) during a period when the $\text{H}_3\text{O}^+/\text{H}_2\text{O}^+$ ratio was low (less than 1). Both mass peaks are well resolved from the background. Error bars shown are counting statistics plus 10 per cent error due to pixel gain uncertainty. The green lines show fits to the mass peaks to determine the total number of detected particles under the peak. The mass scale at the bottom is accurate only to the second decimal place.

the inner region. For example, the average ion energy on 2015 July 6 near 0 UT is about a factor of 2 higher than that on 2015 July 8 near 12 UT. Ions measured by IES are affected by the spacecraft potential (which is typically a few volts negative). Therefore, the energies shown in Fig. 3 are not the true energies of the ions in the coma. However, only the relative ion energy is required here for comparison with the $\text{H}_3\text{O}^+/\text{H}_2\text{O}^+$ ratio and the H_3O^+ signal. H_2O^+ and H_3O^+ are also affected by the spacecraft potential; however, the mass-dependent effects should be small and should not affect the ratio. (For example, a study of the effect of spacecraft potential on the Cassini/Ion and Neutral Mass Spectrometer (INMS) instrument showed that a change in the spacecraft potential essentially causes an increase or decrease in the ion energy independent of mass; Mandt et al. 2012). Finally, the ion energies in Fig. 3 are not used as input to the ionospheric model in Section 5.

Although there is considerable scatter in the $\text{H}_3\text{O}^+/\text{H}_2\text{O}^+$ ratios in Fig. 3, there appears to be a weak anticorrelation between the ratio and the average ion energy. The ratios in the outer region are between 0.1 and 0.8. The ratios in the inner region are generally larger than 1, especially between July 8 and 9, when the ion energy was the lowest for this time period and the ratios were between 1.1 and 50. Gaps in the ion measurements occur when DFMS was not pointed towards nadir, was measuring neutrals, or was not operating because of spacecraft maneuvers. In the second and third panels, there appears to be a similar, weak anticorrelation between the H_3O^+ signal and the average ion energy. That is, the higher the average ion energy, the lower the H_3O^+ signal.

Fig. 4 quantifies the weak anticorrelation between the H_3O^+ signal and the average ion energy. Plotted are the two quantities for the same period from 2015 July 5 to 9 in Fig. 3. The fit through

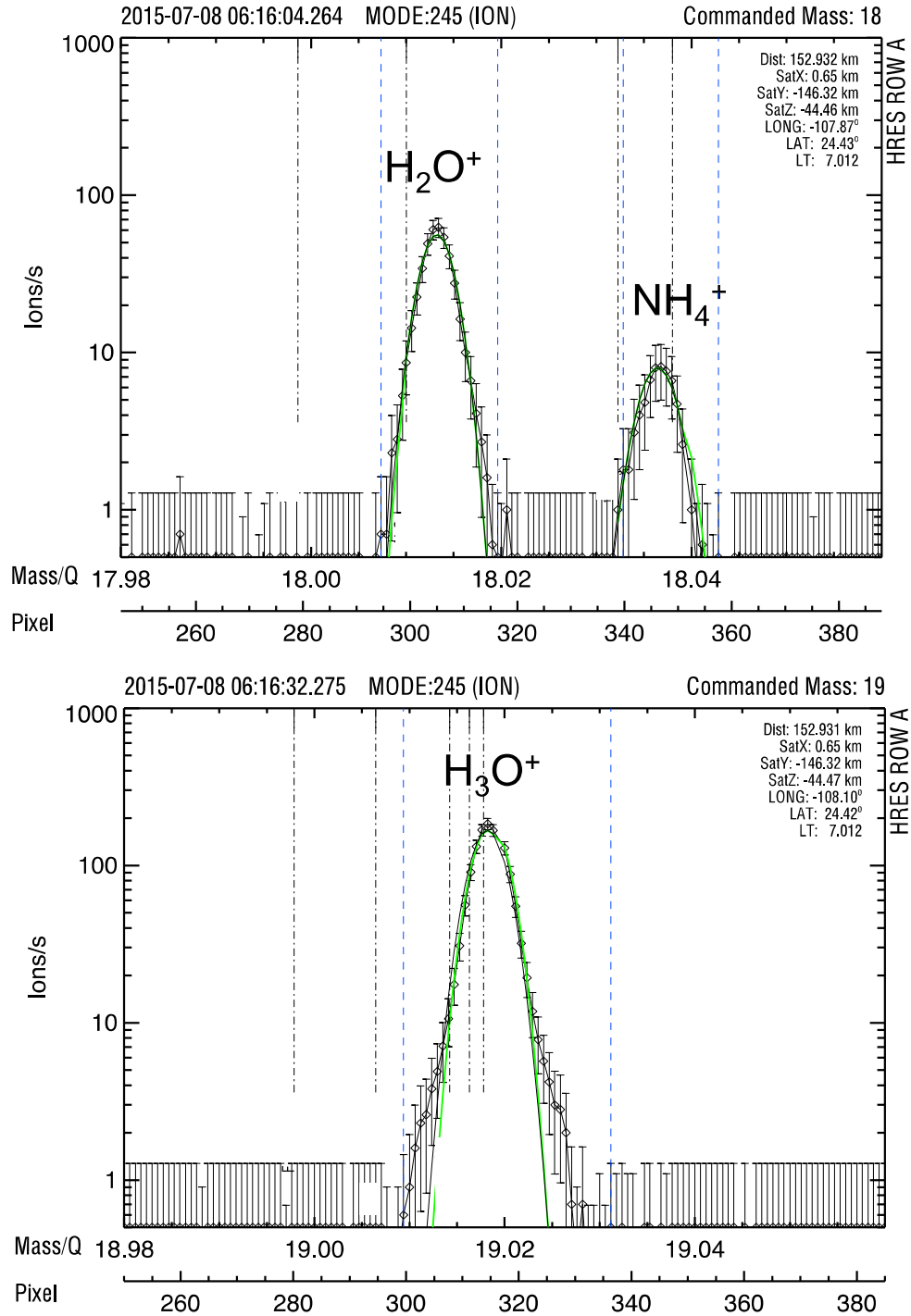


Figure 2. DFMS high-mass resolution ion observations on 2015 July 8 (near perihelion) during a period when the $\text{H}_3\text{O}^+/\text{H}_2\text{O}^+$ ratio was high (>5). The format is the same as in Fig. 1. In addition to H_2O^+ , there is a clearly resolved peak that is identified as NH_4^+ . The double-near-Gaussian peak shape of H_3O^+ is characteristic of DFMS mass spectra.

the points has a correlation coefficient of 0.5, indicating a marginal correlation between the two quantities. The reasons for comparing the H_3O^+ signal and not the $\text{H}_3\text{O}^+/\text{H}_2\text{O}^+$ ratio to the average ion energy are discussed in Sections 5 and 6.

Fig. 5 compares the $\text{H}_3\text{O}^+/\text{H}_2\text{O}^+$ ratios, the H_3O^+ signal and the average ion energies measured by IES during the second interval from 2015 July 21 to 25. Unlike the interval in Fig. 3, the interval in Fig. 5 occurred when the spacecraft was always inside the inner ion

region as identified by Mandt et al. (2016). Similar to the interval in Fig. 3, the average ion energies vary considerably within the inner ion region. For example, on 2015 July 23 at 12 UT, the average ion energy was greater than 10 eV, while on July 25 at about 6 UT, the average ion energy was near 2 eV. At 2 eV, (excluding the effect of the spacecraft potential), water-group ions have already experienced some energization by the pickup process and, as discussed in the next section, this pickup has a significant effect on the ion-neutral

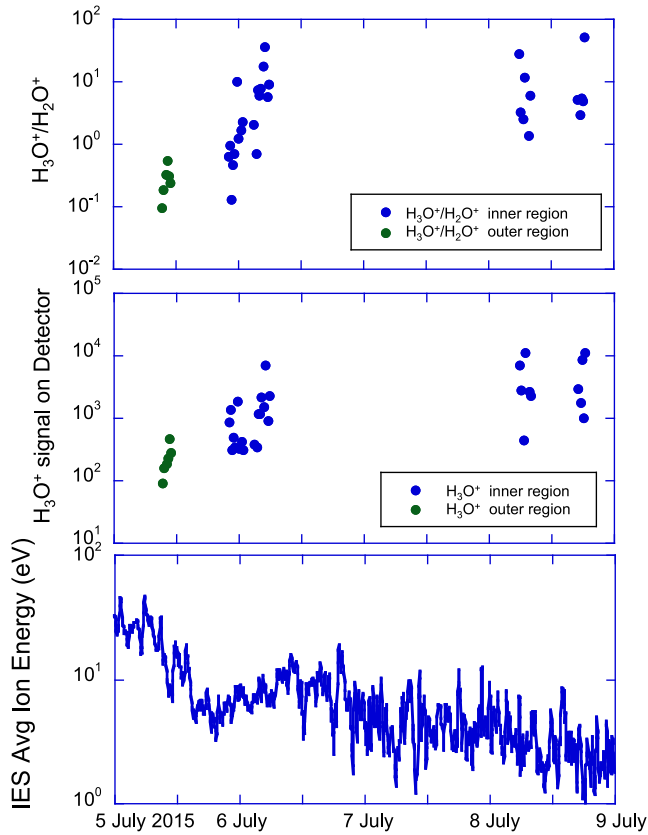


Figure 3. DFMS $\text{H}_3\text{O}^+/\text{H}_2\text{O}^+$ ratio and IES ion energy versus time. At the beginning of the interval, the spacecraft was in the outer region. The ion energy is relatively high and the $\text{H}_3\text{O}^+/\text{H}_2\text{O}^+$ ratio was low. As *Rosetta* enters the inner region, the ion energy decreases and the $\text{H}_3\text{O}^+/\text{H}_2\text{O}^+$ ratio increases above 1. Thus, there is a weak anticorrelation between the ion energy measured by IES and the $\text{H}_3\text{O}^+/\text{H}_2\text{O}^+$ ratio measured by DFMS.

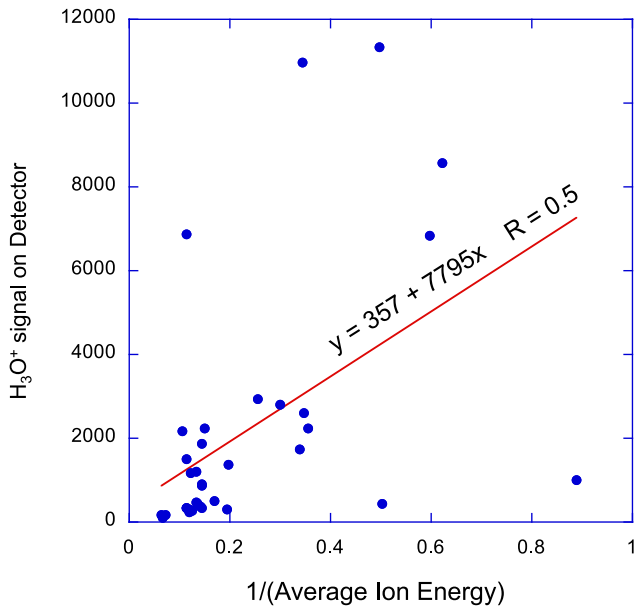


Figure 4. Comparison of $1/(\text{average ion energy})$ and the H_3O^+ signal on the DFMS detector. The two quantities are weakly correlated, with considerable scatter in the H_3O^+ signal.

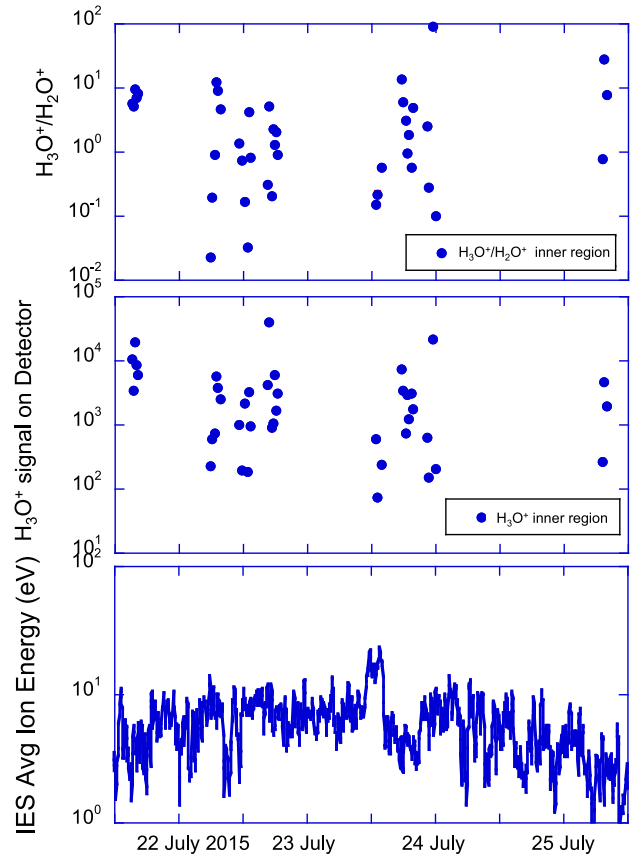


Figure 5. Same as Fig. 3, but for the interval from 2015 July 21–26. *Rosetta* was in the inner region for the entire interval except possibly for the period at 2015 July 23 near 12 UT. Similar to Fig. 3, there is a weak anticorrelation between the ion energy measured by IES and the $\text{H}_3\text{O}^+/\text{H}_2\text{O}^+$ ratio measured by DFMS.

chemistry. Similar to Fig. 3, there appears to be a weak anticorrelation between the $\text{H}_3\text{O}^+/\text{H}_2\text{O}^+$ ratio and the average ion energy. Also similar to Fig. 3, there appears to be a weak anticorrelation between the H_3O^+ signal and the average ion energy. However, the range of ion energies is smaller in Fig. 5 than in Fig. 3 and a correlation plot yields a very poor correlation coefficient.

Figs 6 and 7 investigate other quantities that may correlate with the $\text{H}_3\text{O}^+/\text{H}_2\text{O}^+$ ratio. The top panel of Fig. 6 shows the $\text{H}_3\text{O}^+/\text{H}_2\text{O}^+$ ratio versus local neutral density (measured by COPS) for the first time interval. Although there is considerable variability in the local neutral density, the $\text{H}_3\text{O}^+/\text{H}_2\text{O}^+$ ratio does not correlate with this local density. The lowest ratios are observed at low neutral densities, while the highest ratios are observed at higher neutral densities. The bottom panel of Fig. 6 shows the $\text{H}_3\text{O}^+/\text{H}_2\text{O}^+$ ratio as a function of the sub-spacecraft longitude. All measurements were made between $+20^\circ$ and $+50^\circ$ sub-spacecraft latitude. Generally, negative longitudes have about a factor of 2 higher average ratio than the positive ones and there appears to be a region near -90° longitude where the $\text{H}_3\text{O}^+/\text{H}_2\text{O}^+$ ratio reaches very high values. Since *Rosetta* was in a terminator orbit and northern latitudes were in winter for these intervals near perihelion, the illumination conditions were similar for positive and negative longitudes for the narrow range of sub-spacecraft latitudes considered.

Fig. 7 shows the same comparisons as in Fig. 6 for the second time interval. Similar to the top panel in Fig. 6, the top panel in Fig. 7 shows that the $\text{H}_3\text{O}^+/\text{H}_2\text{O}^+$ ratios are not correlated with the

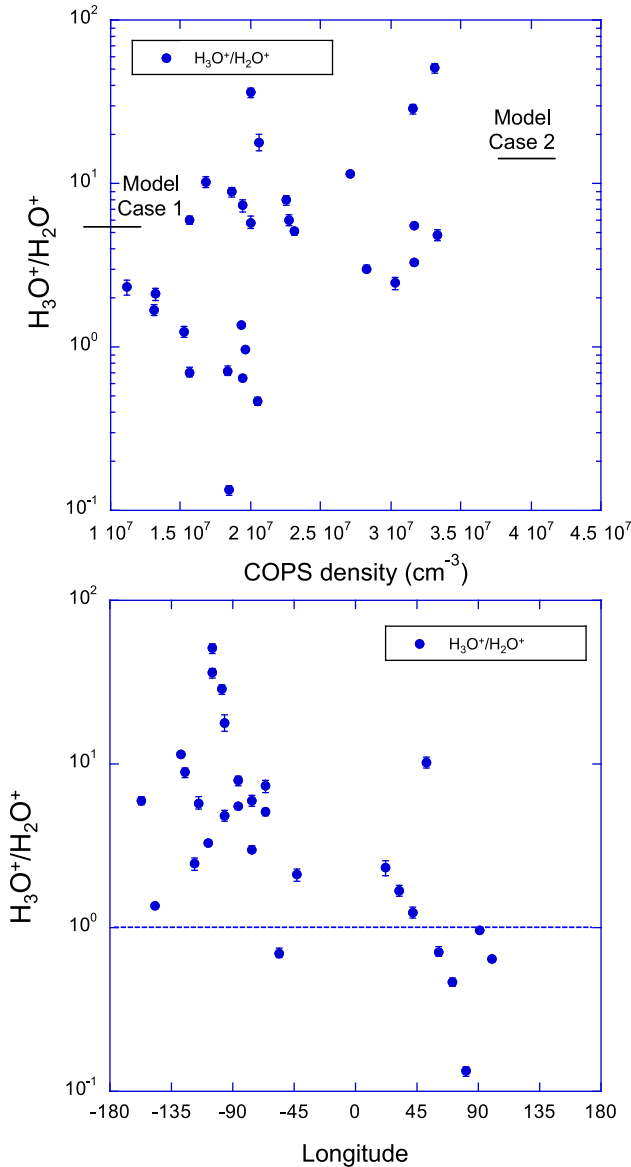


Figure 6. $\text{H}_3\text{O}^+/\text{H}_2\text{O}^+$ ratio versus the local neutral density measured by COPS (top panel) and versus longitude (bottom panel) for the ion observations on 2015 July 5–9. There is modest correlation between the $\text{H}_3\text{O}^+/\text{H}_2\text{O}^+$ ratio and the local neutral density. However, the $\text{H}_3\text{O}^+/\text{H}_2\text{O}^+$ is higher for negative longitudes and there appears to be a ‘hotspot’ near -90° where the ratio becomes very large.

local neutral densities. The bottom panel in Fig. 7 also shows that, as in the first interval, $\text{H}_3\text{O}^+/\text{H}_2\text{O}^+$ ratios were generally higher at negative longitudes. However, the $\text{H}_3\text{O}^+/\text{H}_2\text{O}^+$ ratio does not reach very high values near -90° like in Fig. 6. The sub-spacecraft latitude range for the second interval was between $+2^\circ$ and $+30^\circ$, generally lower than the latitude range for the first interval.

At positive latitudes, the neutral composition of the coma varies with longitude. Fig. 8 shows the time history of neutral H_2O , CO_2 , and CO densities measured by DFMS for two days between the two ion intervals in Figs 3–6 and Table 1. Since the initial encounter with the comet in 2014 August, DFMS observed considerable variation in the neutral density and composition in the coma (Hässig et al. 2015). As seen in Fig. 8, these variations in the coma also occurred near perihelion. The H_2O density measured by DFMS varies by

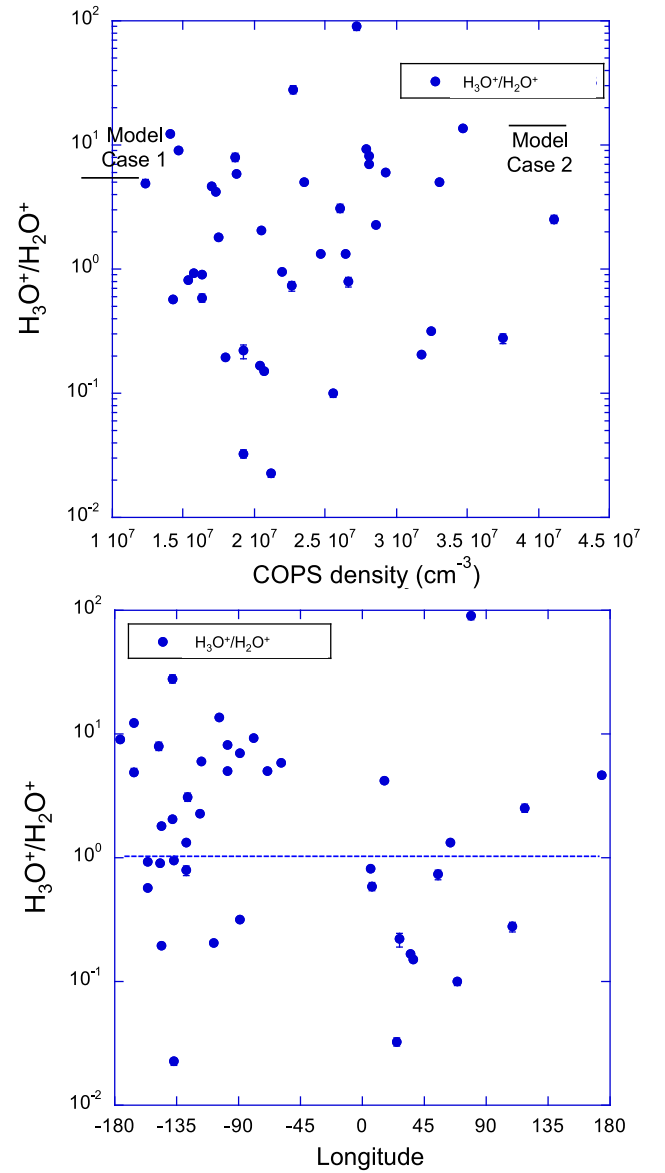


Figure 7. Same as Fig. 6, but for the interval from 2015 July 21–26. Like Fig. 6, there is modest correlation between the $\text{H}_3\text{O}^+/\text{H}_2\text{O}^+$ ratio and the local neutral density. However, the $\text{H}_3\text{O}^+/\text{H}_2\text{O}^+$ is generally higher for negative longitudes although there is no ‘hotspot’ near -90° .

about an order of magnitude with roughly two peaks with equal heights per ~ 12 -h rotation of the nucleus. The first peak occurs near $+90^\circ$ longitude and the second peak occurs near -90° longitude (see the thick and thin vertical dashed lines in Fig. 8). CO_2 and CO peaks in this time series are more difficult to identify, except for two prominent CO_2 peaks on 2015 July 20 near 15 UT and July 21 near 03 UT. At these peaks at negative longitudes, the CO_2 density is about a factor of 2–3 higher than at nearby positive longitudes. Certainly, the H_2O density is always much higher than the CO_2 and CO .

Summarizing the observations: the $\text{H}_3\text{O}^+/\text{H}_2\text{O}^+$ ratio varies over a large range from much less than one to near one hundred in the coma of 67P. Generally, $\text{H}_3\text{O}^+/\text{H}_2\text{O}^+$ ratios and the H_3O^+ signals are small in the outer region identified by relatively higher water-group ion energies. In the inner region, the H_3O^+ signal measured by DFMS appears to be weakly anticorrelated with the average ion energy measured by IES. There is no correlation between the

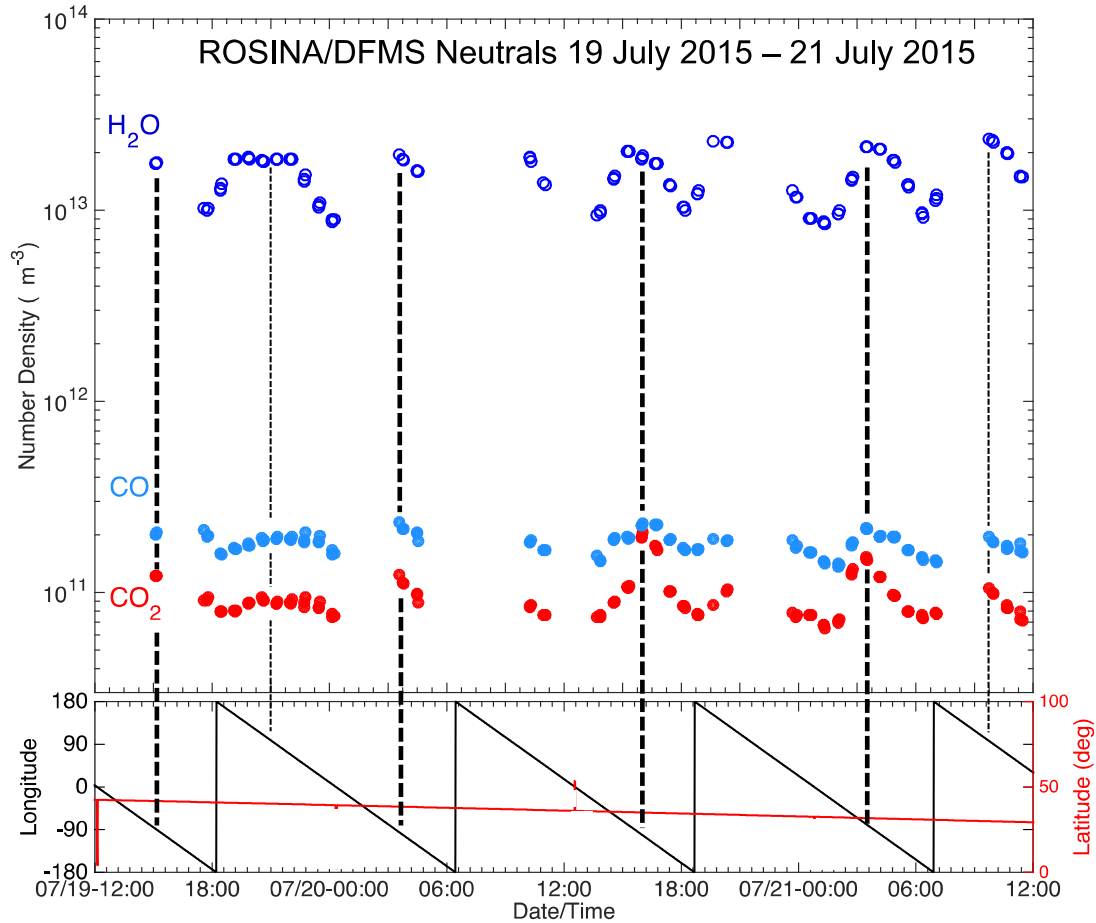


Figure 8. DFMS neutral measurements of H_2O , CO_2 , and CO as a function of time from 2015 July 19 through 21. The H_2O and CO_2 signals have maxima roughly at 6-h intervals (one half a nucleus rotation). For CO , the peaks are much less pronounced and it is usually true that the signal is high for positive longitudes than for negative ones. Thus, there are composition differences between negative and positive longitudes.

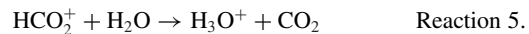
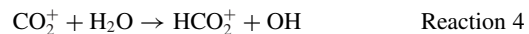
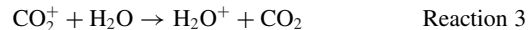
$\text{H}_3\text{O}^+/\text{H}_2\text{O}^+$ ratio and neutral coma density over the range of densities measured by *Rosetta* at ~ 170 km from the comet. However, at positive latitudes, $\text{H}_3\text{O}^+/\text{H}_2\text{O}^+$ ratios are generally higher at negative longitudes than at positive longitudes. Although H_2O is the dominant neutral in the coma at positive latitudes and at all longitudes, the neutral coma composition is different for negative and positive longitudes. In particular, there is often about a factor of 3 more CO_2 at negative longitudes than at positive longitudes. In the inner region, NH_4^+ is regularly observed along with H_2O^+ (see Fig. 2 and Beth et al. 2016). In the Section 5, an ionospheric model is used to determine the relative importance of neutral composition and transport of ions and neutrals away from the nucleus on the $\text{H}_3\text{O}^+/\text{H}_2\text{O}^+$ ratio.

5 MODELLING OF ION-NEUTRAL CHEMISTRY

NH_4^+ in cometary comae is produced through the secondary ion-neutral Reaction 2. Reaction 2 shows that any molecule with proton affinity higher than H_2O will protonate and destroy H_3O^+ . The reaction in Reaction 2 is described as ‘secondary’ because it requires an initial ion-neutral reaction to create H_3O^+ (see Reaction 1). The presence of NH_4^+ in the coma (see Fig. 2 and Beth et al. 2016) indicates that multiple ion-neutral reactions occur. Thus, a simple model that restricts the ion-neutral chemistry to a single reaction

(e.g. the model used in Fuselier et al. 2015) does not describe the ion-neutral interactions for 67P near perihelion.

Multiple ion-neutral reactions also open the possibility that CO_2 may play an important role in the $\text{H}_3\text{O}^+/\text{H}_2\text{O}^+$ ratio. CO_2 is ionized through photoionization to produce CO_2^+ . Additional ion-neutral reactions take two paths:



Because of the multiple reactions, the effect of the CO_2 concentration on the $\text{H}_3\text{O}^+/\text{H}_2\text{O}^+$ ratio must be determined using the full range of ion-neutral reactions in the coma. Furthermore, the importance of this neutral composition must be weighed against transport of ions away from the comet. If the transport is fast enough, then ion-neutral reactions are not frequent enough to produce high amounts of H_3O^+ . This section explores the $\text{H}_3\text{O}^+/\text{H}_2\text{O}^+$ ratio and the relative importance of differences in the coma chemistry and ion transport out of the coma.

The one-dimensional ionospheric model used here is based on the model by Vigren & Galand (2013) and Beth et al. (2016). CO_2 photoionization (see Galand et al. 2016) and associated CO_2

Table 2. Ionospheric simulation input and output.

	Neutral composition (%)	Neutral bulk outflow velocity at the surface (m s^{-1})	Number neutral density at 160 km (cm^{-3}) representative of COPS observations	$\text{H}_3\text{O}^+/\text{H}_2\text{O}^+$ at 160 km
Case 1	96 (H_2O), 1 (CO), 1 (CO_2), 2 (HPA)	400	10^7	5.4
Case 2	Same as case 1	Same as case 1	4×10^7	13.7
Case 3	78 (H_2O), 10 (CO), 10 (CO_2), 2 (HPA)	Same as case 2	Same as case 1	12.1
Case 4	Same as case 1	1000	Same as case 1	4.2

ion-neutral chemistry have been recently added to the model. The ionospheric model computes the number densities of all major ion species versus distance from the comet under solar radiation. It includes photoionization, ion-neutral reactions, electron-ion recombination reactions, and transport.

The neutral number density, bulk velocity, and temperature of the gas are computed assuming adiabatic conditions, with flow expansion and cooling of the gas away from the surface (Cravens, Keller & Ray 1997). The model provides profiles which agree well with those from the kinetic model of Tenishev, Combi & Davidsson (2008). At the surface, the neutral bulk velocity is assumed to be 400 m s^{-1} and the neutral temperature, 200 K. The surface neutral number density is a free parameter adjusted to cover the range of measured values from COPS at 150–175 km. At 1000 km, the neutrals have accelerated up to 950 m s^{-1} and the neutral temperature has decreased down to 3 K, being converted into kinetic energy. This terminal bulk velocity is consistent with the MIRO observations that provided a value of 680 m s^{-1} for a heliocentric distance between 3.5 and 4 au (Gulkis et al. 2015). Higher values of the order of 1000 m s^{-1} are expected near perihelion. The ions are assumed to travel at the same bulk velocity as the neutrals. This assumption is equivalent to assuming that ion acceleration in the coma is weak. In the inner region, this assumption is likely valid. However, as the ions get further away from the comet, they experience acceleration and the net result is that the chemistry is inhibited and H_3O^+ density decreases. Thus, the $\text{H}_3\text{O}^+/\text{H}_2\text{O}^+$ ratio would be an upper limit in regions of significant ion acceleration.

The neutral coma is assumed to be composed of water (96 per cent), CO (1 per cent), CO_2 (1 per cent), and HPA neutrals (2 per cent) for three of the cases and the CO and CO_2 concentrations are increased for one of the cases. The latter influence the $\text{H}_3\text{O}^+/\text{H}_2\text{O}^+$ ratio through the loss of H_3O^+ as shown in Reaction 2 (Vigren & Galand 2013 and Beth et al. 2016).

Neutrals are ionized only through photoionization (i.e. electron impact ionization is excluded from the model). Near perihelion, the prime source of ionization is through solar Extreme Ultra-Violet radiation (Vigren & Galand 2013): Simulations show that, although the outgassing is high, it is likely not high enough to make significant amounts of energetic electrons needed to ionize H_2O . Furthermore, the energetic ($\sim 100 \text{ eV}$) electron population observed by IES is invariant with radial distance outside the diamagnetic cavity (Broiles et al. 2016; Mandt et al. 2016). Therefore, there is no observational evidence indicating that electron impact ionization is important in the coma.

The reaction rates of ion-neutral reactions are dependent on the gas effective temperature, which corresponds to the mass-weighted average of the neutral and ion temperatures. The latter is assumed to be 200 K. The inclusion of electron-ion dissociative recombination requires information on the low-energy electron population, below the energy of *Rosetta*/IES. The reaction rate for dissociative recombination is a function of the electron temperature, which is assumed to be 500 K, which is well below 1 eV and well below what IES can measure.

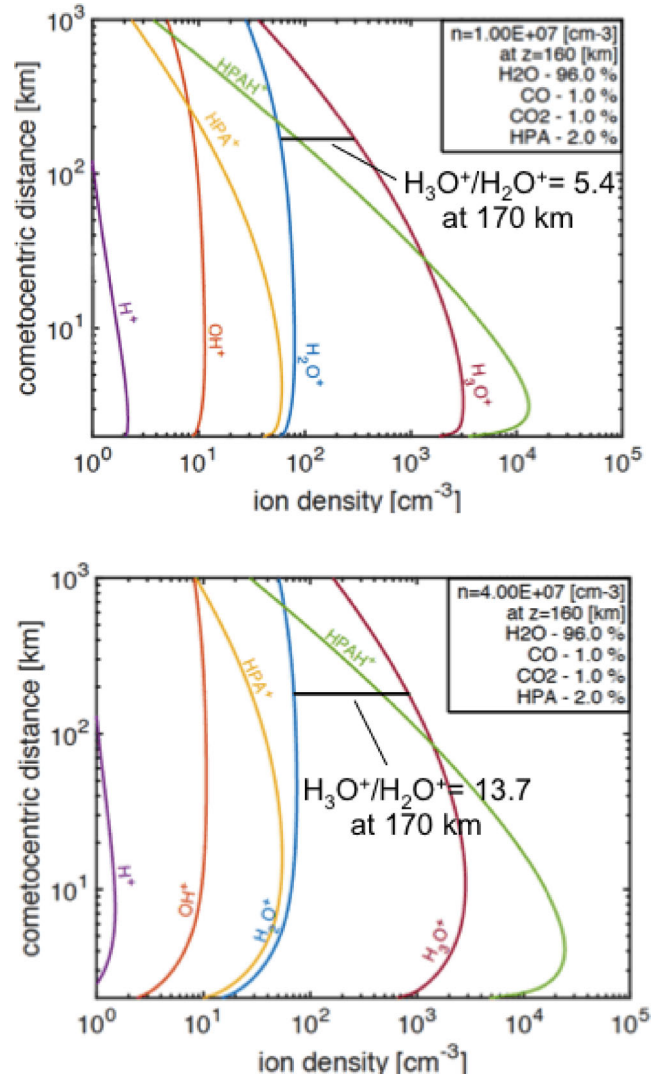


Figure 9. One-dimensional, ionospheric simulations of the ion coma at 67P for a neutral coma composed of 96 per cent of water, 2 per cent of HPA, and 1 per cent of CO and CO_2 , each. The *Rosetta* observations on 2015 July 5–7 and July 21–26 were at a distance between 150 and 175 km from the comet. At this distance, the neutral number density is 10^7 cm^{-3} ($4 \times 10^7 \text{ cm}^{-3}$) for the top (bottom) panel. The low outgassing case 1 (top panel) predicts an $\text{H}_3\text{O}^+/\text{H}_2\text{O}^+$ ratio that is significantly less than the higher outgassing case 2 (bottom panel).

Four modelled comae were simulated. Input parameters along with the derived water ratios for cases 1–4 are given in Table 2, while the calculated ion profiles versus distance from the nucleus for cases 1–4 are shown in Figs 9 and 10. Cases 1, 3 and 4 assume a neutral number density at the surface such that the density at 160 km is 10^7 cm^{-3} . While, for case 2, the density at 160 km is $4 \times 10^7 \text{ cm}^{-3}$. This is representative of the low (high) outgassing

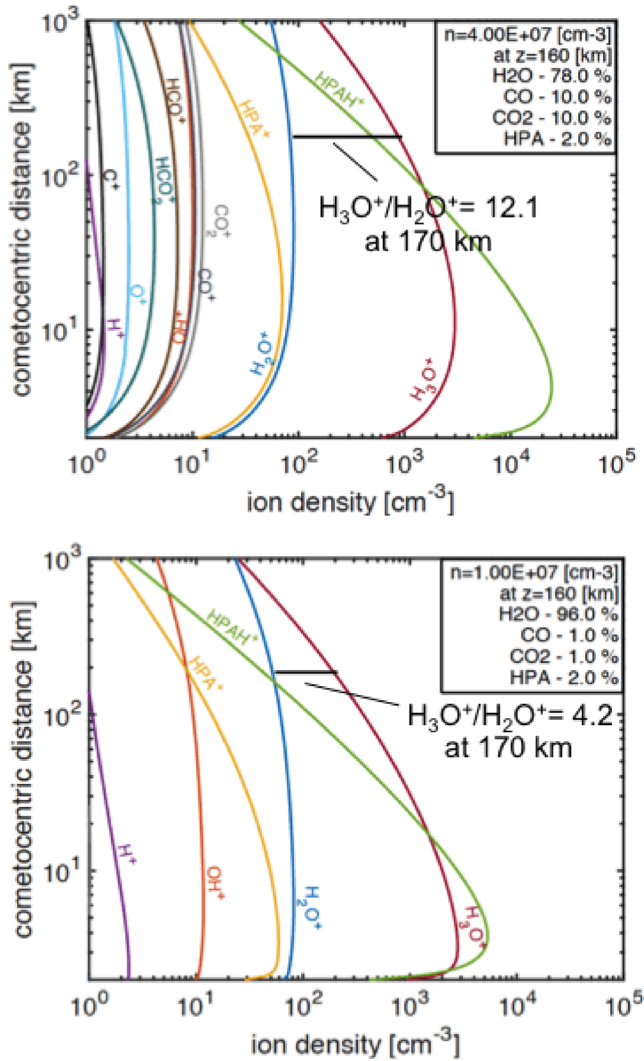


Figure 10. (Top) Same as Fig. 9 bottom, but with a different composition for the coma, 78 per cent (H_2O), 2 per cent (HPA), 10 per cent (CO), and 10 per cent (CO_2). (Bottom) Same as Fig. 9 top but with a neutral outflow bulk velocity of 1000 m s^{-1} . The composition change had a small effect on the $\text{H}_3\text{O}^+/\text{H}_2\text{O}^+$ ratio compared to the increase in the outflow bulk velocity.

rate observed by COPS in Fig. 6. Cases 1 and 2 represent baseline conditions of a H_2O -dominated coma. Case 3 shows the effect of a change in composition of the coma and case 4 shows the effect of a change in transport time-scale for the ions. For low CO and CO_2 in the coma (Figs 9 and 10, top), only H_3O^+ , H_2O^+ , OH^+ , and H^+ are shown. For high CO and CO_2 (Fig. 10, top), additional carbon-bearing ions are shown.

Fig. 9 shows the simulations for the baseline cases. With no acceleration of the ions – beyond the gas expansion – photoionization and ion-neutral chemistry can occur. As a result, H_2O^+ is in photochemical equilibrium, while H_3O^+ is lost from reactions with HPA neutrals as well as through transport (which becomes increasingly dominant with higher cometocentric distance). At the location of *Rosetta* (150–175 km), H_3O^+ remains one of the dominant species and the water ratio is well above 1. With increased outgassing rate, the chemistry is enhanced. As a result, the high outgassing case 2 (bottom panel) shows a higher $\text{H}_3\text{O}^+/\text{H}_2\text{O}^+$ ratio than the lower outgassing case 1 (top panel) (see also Table 2).

Fig. 10 (top) shows ion profiles from case 3, which is identical to case 2 (Fig. 9, bottom) except with a different composition: 78 per cent (H_2O), 2 per cent (HPA), 10 per cent (CO), and 10 per cent (CO_2). CO and CO_2 volume mixing ratios have been enhanced, inducing a reduction in the volume mixing ratio of water. The increase on CO and CO_2 volume mixing ratios is extreme, as compared with composition shown in Fig. 8. Nevertheless, the change in $\text{H}_3\text{O}^+/\text{H}_2\text{O}^+$ ratio remains modest (12 per cent decrease). The $\text{H}_3\text{O}^+/\text{H}_2\text{O}^+$ ratio is therefore essentially independent of the abundance of neutral CO and CO_2 in the coma with the volume mixing ratios observed during this period (1 to < 10 per cent).

Fig. 10 (bottom) shows profiles from case 4, which is identical to case 1 (Fig. 9, top) except with an artificially enhanced neutral bulk velocity u_0 at the surface. This case tests the sensitivity of the $\text{H}_3\text{O}^+/\text{H}_2\text{O}^+$ ratio with transport. For $u_0 = 1000 \text{ m s}^{-1}$, the terminal velocity is 1300 m s^{-1} , which represents a 37 per cent increase compared with case 1. With increased bulk velocities, the ion transport time-scales are reduced and chemistry is inhibited. As a result, the $\text{H}_3\text{O}^+/\text{H}_2\text{O}^+$ ion ratio decreases by 22 per cent. Though due to the modest acceleration, the decrease in the water ion ratio is small and does not compare well with observations. However, this case demonstrates that acceleration of the ions decreases the ion ratio. With the large-velocity increase observed by IES, the water ion ratio is expected to reach significantly lower values.

The values of the $\text{H}_3\text{O}^+/\text{H}_2\text{O}^+$ ratios given in Table 2 are consistent with the upper values observed (see Figs 6 and 7). The model does not explain lower observed water ratio values, which most likely result from significant acceleration of ions not captured in the model. Variations from the modelled values could also be due to a change in composition (e.g. HPA neutrals), ion and electron temperatures, and activity level. However, the largest effect comes from acceleration of ions as they propagate away from the nucleus.

6 CONCLUSIONS

The outer and inner regions identified in the ion observations at 67P have similarities in the ion energies, and magnetic field magnitudes to the region outside and within the ion pile-up region observed at comet Halley (Mandt et al. 2016). Observations presented here suggest that the $\text{H}_3\text{O}^+/\text{H}_2\text{O}^+$ ratio behaves similarly in these regions at the two comets. The $\text{H}_3\text{O}^+/\text{H}_2\text{O}^+$ was generally less than one in the outer region at 67P and appears to be weakly anticorrelated with total ion energy in the inner region. Similarly, the $\text{H}_3\text{O}^+/\text{H}_2\text{O}^+$ ratio was less than one outside the ion pile-up region at comet Halley and increased to a peak of 5–6 inside the region. In Fig. 5, the H_3O^+ signal is correlated with the ion energy because this ion density varies considerably with distance from the nucleus and is sensitive to acceleration (Figs 9 and 10, top). The weak anticorrelation between average ion energy and H_3O^+ signal therefore highlights the importance of the acceleration. When ions are travelling faster, then there is reduced time for chemical reactions and the H_3O^+ signal and the $\text{H}_3\text{O}^+/\text{H}_2\text{O}^+$ ratio are reduced.

At 67P, the $\text{H}_3\text{O}^+/\text{H}_2\text{O}^+$ ratio was also observed to vary with longitude and there is often about a factor of 3 more CO_2 at negative longitudes than at positive longitudes (Fig. 8). Although H_2O is the dominant neutral, this CO_2 variation with longitude suggests that the $\text{H}_3\text{O}^+/\text{H}_2\text{O}^+$ ratio varies with neutral composition. However, ionospheric modelling shows that CO and CO_2 have a much weaker effect on the $\text{H}_3\text{O}^+/\text{H}_2\text{O}^+$ ratio. Furthermore, the effect is in the opposite direction from the observations that the CO_2 density is higher at negative longitudes than at positive ones, yet the $\text{H}_3\text{O}^+/\text{H}_2\text{O}^+$ ratio is higher at negative longitudes. Thus, it is likely

that the $\text{H}_3\text{O}^+/\text{H}_2\text{O}^+$ ratio changes in the inner and outer regions because the ion acceleration is different. In particular, a higher effective outflow speed for the ions implies more rapid transport away from the comet before ion-neutral reactions can create H_3O^+ . The very low $\text{H}_3\text{O}^+/\text{H}_2\text{O}^+$ ratios at the *Rosetta* distance from the nucleus must be due to some ion acceleration, though it is also sensitive to the mixing ratio of HPA (Beth et al. 2016). While the model is suitable for explaining the high ratios observed in the inner region, observations suggest the need for a kinetic model where the ions are picked up by the convection electric field to describe the outer region. Including extended sources (from dust) may also have important effects on the $\text{H}_3\text{O}^+/\text{H}_2\text{O}^+$ ratio.

Finally, it appears justified to not consider the effects of the energetic electron population on the $\text{H}_3\text{O}^+/\text{H}_2\text{O}^+$ ratio. An energetic (~ 100 eV) electron population with sufficient density changes the production of H_2O^+ and affects the ion-neutral chemistry in the coma. However, modelling indicates that the electron density near perihelion was insufficient for electron impact ionization to be important (Vigren & Galand 2013) and the energetic (~ 100 eV) electron population appears invariant of radial distance outside the diamagnetic cavity of 67P (Broiles et al. 2016; Mandt et al. 2016). Thus, there was no major change in the electron impact ionization in the transition between the regions. There was a decrease in the cold (few eV) electron density from the inner to the outer region as expected when the velocities increase due to ion pickup and these cold electrons are important for dissociative recombination in the coma. However, the lack of a change in the energetic electron density indicates that photoionization is still the dominant means for producing ions in the coma.

ACKNOWLEDGEMENTS

The *Rosetta*/ROSINA and IES teams consist of many individuals who worked over a period of more than 20 yr to achieve the spectacular successes from the *Rosetta* mission encounter with comet 67P. The authors are deeply indebted to these individuals. Research at Southwest Research Institute was conducted under subcontract Number 1496541 from the Jet Propulsion Laboratory. Work at the Belgian Institute for Space Aeronomy is supported by the Belgian Science Policy office through Prodex/ROSINA PRODEX Experiment Arrangement 90020. Work at Imperial College London is supported by the Science and Technology Facilities Council (STFC) of the UK under grants ST/K001051/1 and ST/N000692/1. Work at Laboratoire atmosphères, milieux, observations spatiales and Institut de Recherche en Astrophysique et Planétologie is supported by funding from Centre national d'études spatiales. Work at Lockheed Martin Advanced Technology Center was performed under subcon-

tract 1436821. Work in Bern is funded by the Canton of Bern, the Swiss National Science Foundation and by the space agency Programme de Développement d'Expériences scientifiques program. Work at the Swedish Institute of Space Physics is supported by the Swedish National Space Board under contract number 166/14.

REFERENCES

- Altwegg K. et al., 1993, *A&A*, 279, 260
 Balsiger H. et al., 1986, *Nature*, 321, 330
 Balsiger H. et al., 2007, *Space Sci. Rev.*, 128, 745
 Behar E., Nilsson H., Wieser G. S., Nemeth Z., Broiles T. W., Richter I., 2016, *Geophys. Res. Lett.*, 43, 4
 Beth A. et al., 2016, *MNRAS*, in press
 Broiles T. W. et al., 2015, *A&A*, 583, A21
 Broiles T. W. et al., 2016, *MNRAS*, in press
 Burch J. L., Goldstein R., Cravens T. E., Gibson W. C., Lundin R. N., Pollock C. J., Winningham J. D., Young D. T., 2007, *Space Sci. Rev.*, 128, 697
 Burch J. L., Cravens T. E., Llera K., Goldstein R., Mokashi P., Tzou C.-Y., Broiles T., 2015, *Geophys. Res. Lett.*, 42, 5125
 Coates A. J., 1997, *Adv. Space Res.*, 20, 255
 Cravens T. E., Keller C. N., Ray B., 1997, *Planet. Space Sci.*, 45, 889
 Fougere N. et al., 2016, *MNRAS*, in press
 Fuselier S. A. et al., 2015, *A&A*, 583, A2
 Galand M. et al., 2016, *MNRAS*, in press
 Goetz C. et al., 2016, *A&A*, 588, A24
 Gringauz K. I., Verigin M. I., Richter A. K., Gombosi T. I., Szegő K., Tatrallyay M., Remizov A. P., Apathy I., 1986, *ESLAB Symposium on the Exploration of Halley's Comet*, Vol. 250, p. 93
 Gulks S. et al., 2015, *Science*, 347, 6220
 Hansen et al., 2016, *MNRAS*, in press
 Hässig M. et al., 2015, *Science*, 347, aaa0276
 Mandt K. E., 2016, *MNRAS*, 462(Supp), S9
 Mandt K. E. et al., 2012, *J. Geophys. Res.*, 117, E10006
 Neubauer F. M. et al., 1986, *Nature*, 321, 352
 Richardson J. D., Paularena K. I., Gazis P. R., 1995, *NASA Ames Solar Wind 8 Conference Proceedings*, p. 90
 Schwenn R., Ip W. H., Rosenbauer H., Balsiger H., Bühler F., Goldstein R., Shelley E. G., 1988, *Exploration of Halley's Comet*. Springer, Berlin Heidelberg, 160
 Tenishev V., Combi M., Davidsson B., 2008, *ApJ*, 685, 659
 Vaisberg O. L., Smirnov V. N., Gorn L. S., Iovlev M. V., 1987, *Kosm. Issled.*, 25, 867
 Vigren E., Galand M., 2013, *ApJ*, 771, 1
 Wurz P. et al., 2015, *A&A*, 583, A22

This paper has been typeset from a Microsoft Word file prepared by the author.